OATAO
Open Archive Toulouse Archive Ouverte

Open Archive Toulouse Archive Ouverte (OATAO)

OATAO is an open access repository that collects the work of Toulouse researchers and makes it freely available over the web where possible

This is an author's version published in: http://oatao.univ-toulouse.fr/28308

Official URL: https://doi.org/10.1016/j.jeurceramsoc.2021.07.014

To cite this version:

Rousselle, Mélanie and Ansart, Florence and Hérisson de Beauvoir, Thomas and Fradet, Guillaume and Estournès, Claude *Phase evolution and sinterability of lanthanum phosphate – Towards a below 600 °C Spark Plasma Sintering.* (2021) Journal of the European Ceramic Society, 41 (14). 7261-7268. ISSN 0955-2219

Any correspondence concerning this service should be sent to the repository administrator: tech-oatao@listes-diff.inp-toulouse.fr

Phase evolution and sinterability of lanthanum phosphate – Towards a below 600 °C Spark Plasma Sintering

Mélanie Rousselle [a,b], Florence Ansart [a], Thomas Hérisson de Beauvoir [a], Guillaume Fradet [b], Claude Estournès [a,*]

[a] Université de Toulouse, CIRIMAT, CNRS INPT UPS, Université Paul Sabatier, 118 route de Narbonne, 31062, Toulouse cedex 9, France
[b] SAFRAN Aircraft Engines, 2 Rue Henri Auguste Desbruères, 91100, Corbeil-Essonnes, France

ARTICLE INFO

Keywords:
Lanthanum phosphates
Spark Plasma Sintering
Structure
Microstructure
Micro-hardness

ABSTRACT

Lanthanum phosphate, due to its interesting thermal and mechanical properties is a widely studied material for refractory applications. Sintering processes have already been proposed to densify this material and drive its microstructure. Inspired by recent progress on low temperature sintering, we investigate a low temperature Spark Plasma Sintering (LowT-SPS) using hydrated precursor. First, lanthanum phosphate thermal behaviour was studied using TGA/DTA and XRD analysis on various heat-treated powders. Their SPS behaviour were explored by *in situ* dilatometry measurements. As hydrated precursor showed a low temperature densification, samples were sintered at temperatures from 160 °C to 350 °C under 400 MPa. Even if dense and nano-scaled microstructures were obtained, a residual hydration was observed. Finally, a well densified and fine-grained monazite type lanthanum phosphate was obtained at 550 °C and under 200 MPa. Its mechanical properties are then compared to conventional and Spark Plasma Sintered materials.

1. Introduction

Lanthanum phosphates are widely studied as refractory ceramics for applications in the fields of energy production (thermal, nuclear industries) and transportation (automotive, aeronautical and space industries) [1]. $LaPO_4$ has a high melting point of 2072 °C [2], a chemical inertness up to 1600 °C [3,4] and a low thermal conductivity between 1.2 and 3.6 $W.m^{-1}.K^{-1}$ [4] that makes it an interesting thermal insulating material [1,5,6]. Moreover, monazite type $LaPO_4$ has an interesting brittle behaviour characterized by Vickers micro-hardness in the order of 5 GPa and fracture toughness of around 1 $MPa.m^{1/2}$ [1]. Its pseudo-lamellar structure allows high temperature dislocation propagation and makes it a deformable refractory material [5]. For these reasons, it is widely proposed as promising candidate for the elaboration of machinable refractory material [5,7,8]. Lanthanum phosphate is usually obtained by co-precipitation or sol-gel synthesis, in a hydrated form (i.e. $LaPO_4.xH_2O$) with a rhabdophane structure [2,5]. Synthesis is then, most of the time, followed by a calcination step to induce the high temperature monazite phase crystallisation [9]. As most refractories, the monazite type $LaPO_4$ is sintered above 1000 °C [5,9]. Calcination followed by compaction and conventional high temperature sintering makes elaboration of lanthanum phosphate a multi-step and energy consuming process. Moreover, thermal dilatation constraints induced by high temperature limit multi-layered coatings co-firing.

Recently, the development of extremely low temperature sintering techniques has proved their efficiency for the sintering of a wide range of materials below 400 °C [10], down to room temperature [11]. The general mechanisms, although uncertain [12], proceed through pressure solution creep achieved under high pressure (usually from 100 MPa to 1 GPa). The use of a liquid phase as a solvent for dissolution-transport-precipitation steps offers a wide range of possibilities for controlling reactivity and sintering. This way, sintering process extended to new types of materials, some of which couldn't withstand high temperature sintering [13–16]. Various materials families were densified, including sulphate [17], carbonate [18], hydroxide [19], and phosphate [20].

Reactive sintering was developed for the preparation of some materials, implying a precursor decomposition (hydrated phase, hydroxide) during the sintering process to allow their densification. This was successfully applied to thermally fragile phases [17,21,22] and chemically inert materials [19,23].

Although various sintering approaches were developed to achieve

* Corresponding author.
E-mail address: estournes@chimie.ups-tlse.fr (C. Estournès).

https://doi.org/10.1016/j.jeurceramsoc.2021.07.014

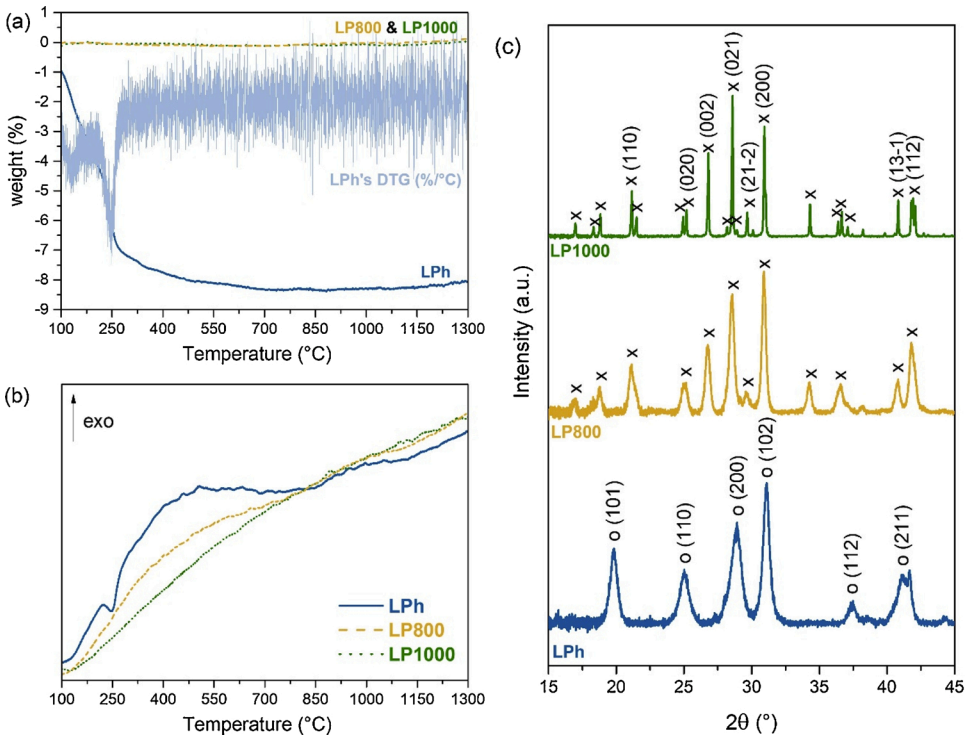


Fig. 1. TGA (a); DTA (b) and XRD (c) characterization of LPh, LP800 and LP1000.

low temperature sintering, the general trend consists in applying a mild temperature and high pressure on a sample made of pure or slightly wetted solid. This way, we used the SPS equipment at low temperature and high pressure to achieve low temperature sintering of lanthanum phosphate in similar temperature conditions.

2. Material and method

A commercial lanthanum (III) phosphate hydrate ($LaPO_4$. xH_2O) powder was purchased from Alfa Aesar and named LPh. 800 and 1000 °C heat treatments during 2 h in air were performed on these raw powders using a Nabertherm oven. Calcined powders are named in the following LP800 and LP1000, respectively. Thermal behaviour of raw powders is first studied using TGA/DTA analyses with a SETARAM (TAG16) equipment in 100–1400 °C range with a 10 °C/min heating rate in air.

Sintering is carried out using both a Dr. Sinter 2080 unit, SPS Syntex Inc., Japan and a Dr. Sinter 632Lx, Fuji Electronic Industrial CO, Japan, available at the Plateforme Nationale de Frittage Flash located at the Université Toulouse 3 Paul Sabatier. Spark Plasma Sintered pellets are obtained by loading powders into a Ø 20 mm graphite die lined with a 0.2 mm graphite foil (PERMA-FOIL®Toyo Tanso). Temperature is first stabilized at 600 °C for 5 min with a heating rate of 200 °C/min to reach the pyrometer threshold detection. Temperature is raised to 1000 °C at 100 °C/min then to 1150 °C at 50 °C/min. Pressure is increased along with the temperature to 100 MPa. Sintering dwell lasts 10 min. Finally, temperature and pressure are both released at the same time in 20 min.

Comparatively, low temperature sintered pellets are obtained by loading raw hydrated precursor into a Ø 20 mm tungsten carbide die lined with a 0.2 mm graphite paper. Pressure of 400 MPa was applied in 5 min at 25 °C before raising the temperature at 50 °C/min up to set-points of 160 °C, 200 °C, 260 °C and 350 °C, respectively, at which it is maintained for 10 min. Temperature is measured with a thermocouple set in the die wall, near the powder.

Crystalline phases of raw powders, heat treated powders and sintered pellets have been determined by X-ray diffraction using a D4 Endeavor Brucker AXS. Measurements are performed at room temperature using Cu Kα1 and Kα2 radiation with a Bragg-Brentano geometry with $10° < 2\theta < 45°$. Secondary electron micrographs were obtained using a field emission-gun scanning electron microscopy (Quanta 250 FEG FEI) available at Centre de Microcaractérisation Raimond Castaing, UMS 3623, Université de Toulouse. Acquisition parameters were 20 kV using a 10 mm working distance on 8 nm Pt covered fracture surfaces. Finally, mechanical properties were evaluated by micro-hardness device using Vickers indentation (Hv0.3) on a Mitutoyo HM200 equipment.

3. Results and discussions

Thermal behaviour of lanthanum phosphate is studied to identify dehydration and phase evolution from rhabdophane to monazite structure. Precursors hydration and crystallisation influences on sintering are investigated using Spark Plasma Sintering *in situ* dilatometry measurements. As hydrated precursor showed a low temperature densification, investigation on its sintering behaviour is complemented with dilatometry measurement from room temperature to 400 °C. Phase crystallisation, microstructures and residual hydration of lanthanum phosphates sintered from 160 °C to 350 °C are carried out to understand their impact on micro-hardness. Finally, micro-hardness of a well densified and fine-grained lanthanum phosphate sintered at 550 °C is compared to conventionally sintered and high temperature Spark Plasma Sintered samples.

3.1. Powder characterization

Phase stability and purity of the purchased hydrated $LaPO_4.xH_2O$ (named LPh) were controlled by TGA/DTA measurements on a 100–1400 °C temperature range. Results are given in Fig. 1 (a) and (b). Final weight loss of 7.9 % occurs at three various temperatures correlated with endothermic events. Between 110 °C and 150 °C, LPh loses 4 wt.%, then 2.9 wt.% at 260 °C, and finally 1 wt.% is progressively lost between 300 °C and 500 °C. The first endothermic weight loss is usually attributed to physisorbed water evaporation and second one to

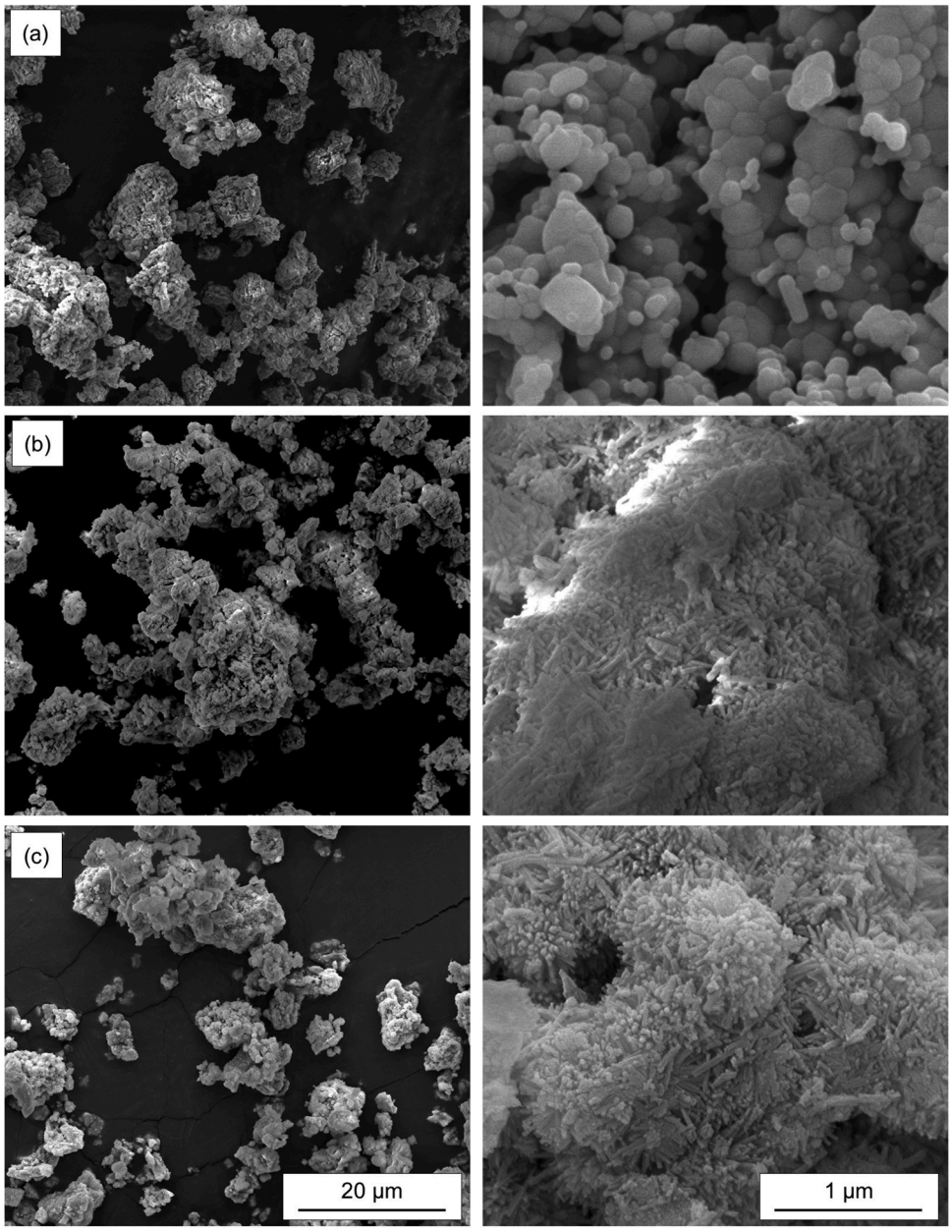


Fig. 2. SEM micrographs of (a) 1000 °C, (b) 800 °C heat treated and (c) as received $LaPO_4.xH_2O$.

chemisorbed water [2,24–27]. The third one must correspond to the end of chemisorbed water loss [2] along with loss of organic pollutant resulting from the synthesis [26]. The 2.9 wt.% to 3.9 wt.% loss of chemisorbed water implies the expected composition of $LaPO_4 \cdot xH_2O$ (x = 0.4 to 0.5) [2,24–27].

From 500 °C to 1400 °C, no more weight loss is observed in LPh thermogravimetric curve. Moreover, no other well defined peak seems present on LPh DTA curve. The lack of thermic event at 950 °C and 1260 °C, usually attributed to the formation and decomposition of $La(PO_3)_3$ phosphate compound [2], attests the lanthanum phosphate phase purity and its correct 1:1 La:P stoichiometry. However, the lack of an exothermic peak on the 500–1400 °C range is inconsistent with the crystallization of monazite phase usually observed with a sharp exothermic peak at 480 °C [28], 550 °C [26] or 700–750 °C [2,24]. DTA curves of LPh and LP800 exhibit exothermic event on the wide range of 150–825 °C which is not observed for LP1000. Thus, this wide exothermic event can be explained by the monazite crystallisation which must be progressive.

To confirm crystallization of monazite along with increasing temperatures, XRD analysis is proceeded on raw and heat treated powders. Peaks of LPh powder diffraction pattern on Fig. 1(c) are indexed by the hexagonal hydrated $LaPO_4 \cdot 0.5H_2O$ rhabdophane phase [2]. It exhibits wide peaks suggesting submicronic crystallite size and a thinner one (102) that suggests a preferred orientation of the crystallites. LP800 and LP1000 diffraction pattern correspond to dehydrated $LaPO_4$ monazite structure [2]. However, XRD pattern exhibits wider diffraction peaks for LP800 as compared to LP1000. One can note that transition occurs below 800 °C but may not be fully complete at this temperature explaining wider diffraction peaks and exothermic event on the LP800 DTA curve.

XRD results are complemented by microstructural observations on powders SEM micrographs. The hydrated phase (LPh), is made of agglomerated nano-rods of 150 ± 50 nm length and 26 ± 3 nm thickness. That is consistent with the submicronic and preferred orientation suggested by diffraction peaks width. On the contrary, LP1000 is formed by 250 ± 50 nm spherical particles, resulting in thin diffraction peaks.

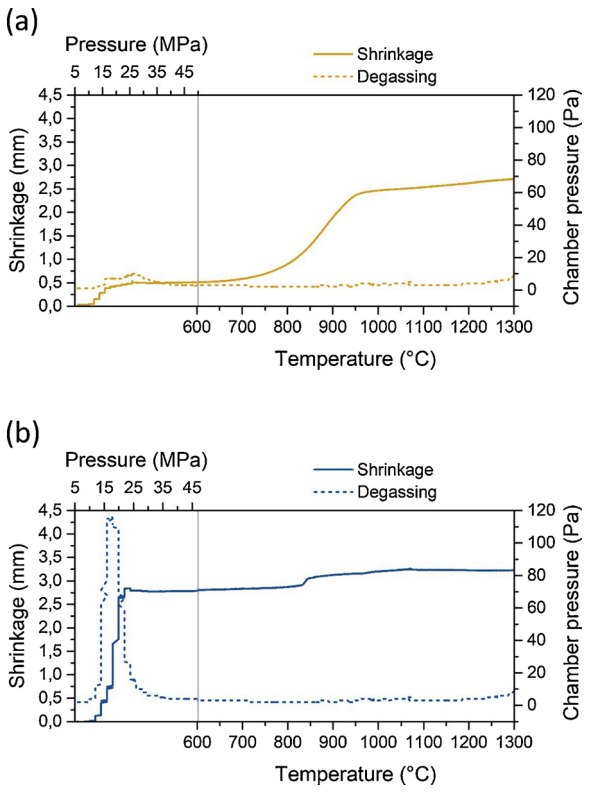


Fig. 3. High temperature dilatometry test on Spark Plasma Sintering equipment of (a) LP800 and (b) LPh.

LP800 microstructure seems to be an intermediate between LPh and LP1000. Q. Zheng *et al.* [9] ascribed this microstructural evolution to the fragmentation of nano-rods into nano-spheres, further growing above 1000 °C (Fig. 2).

3.2. *Spark Plasma Sintering behaviour of various $LaPO_4$ precursors*

These progressive dehydration and phase evolution of $LaPO_4 \cdot xH_2O$ influence on SPS behaviour were investigated. Both hydrated LPh and partially inert LP800 precursors are compared using SPS *in situ* dilatometry measurements. In a first step, 50 MPa pressure is applied in 5 min under dynamic vacuum and temperature is raised and stabilized from room temperature to the first temperature detected by the pyrometer: 600 °C. The second step corresponds to the dilatometry measurement: temperature is raised up to 1300 °C with a 40 °C/min heating rate under constant 50 MPa pressure. Chamber pressure and shrinkage of LP800 and LPh (respectively, on Fig. 3(a) and (b)) are reported as a function of pressure for step 1 and as function of temperature for step 2.

LP800 powder shrinkage (Fig. 3 (a)) shows a main event between 650 °C and 1000 °C, centred at 815 °C. This corresponds to an important 2 mm displacement without degassing phenomenon. It is likely to be monazite phase sintering. According to D. Bregiroux *et al.* [29], pressureless sintering of calcined powder usually takes place between 900 °C and 1160 °C. However, the higher applied pressure (50 MPa) in our experiment must explain such lowered sintering temperature. Below 600 °C, during the first heating and pressure ramp, a first slight gas release occurs, linked with a small shrinkage. Given the previous observations (part I) these events can be attributed to, respectively, degassing of residual surface hydration and particle rearrangement.

LPh behaviour is more complex than LP800. First, an important gas release is observed (Fig. 3 (b)) during pressure ramp (below 600 °C). It is attributed to LPh powder dehydration. This gas release comes along with an important shrinkage on Fig. 3 (b). This might either be attributed to water loss, phase transformation from rhabdophane to monazite

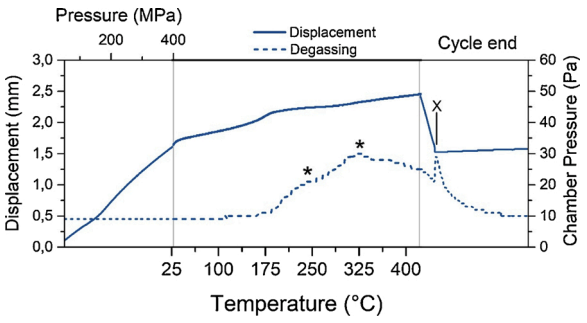


Fig. 4. Low temperature dilatometry test on Spark Plasma Sintering equipment, (a) SPS chamber pressure and (b) thickness shrinkage.

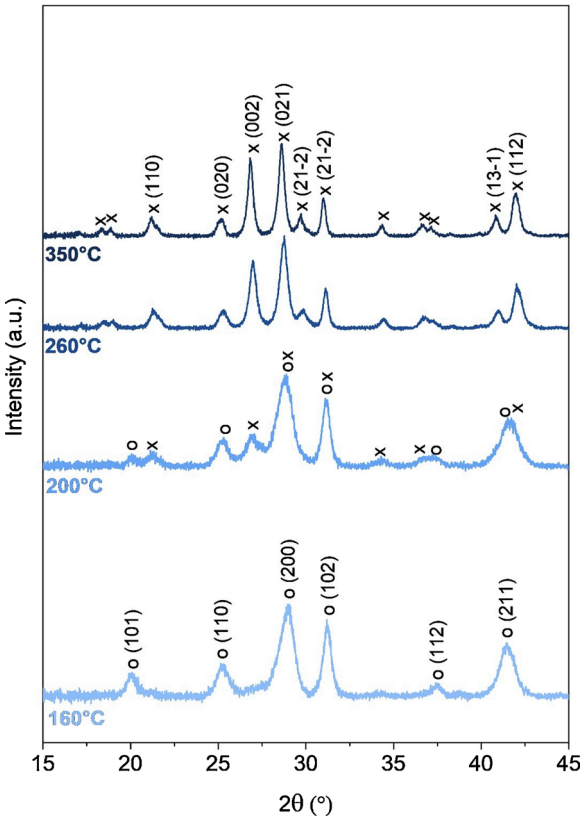


Fig. 5. X-Ray diffraction of low temperature sintered $LaPO_4 \cdot xH_2O$.

structure or particles rearrangement. The coexistence of both high heating and pressure ramp during the first step makes each phenomenon contribution difficult to dissociate. Finally, a slight volume shrinkage without gas release takes place at 815 °C, it must be attributed to monazite sintering as observed for LP800.

This last observation highlights an interesting difference on volume shrinkage behaviour of the dehydrated-monazite phase (LP800) and the hydrated-rhabdophane phase (LPh). LP800 shrinkage ranges from 650 °C to 1000 °C while LPh shrinkage occurs below 600 °C along with phase transformation and dehydration. Using a hydrated precursor seems to allow the access to a reactive sintering taking place at lower temperature and facilitated by applied pressure.

3.3. *Low temperature Spark Plasma Sintering behaviour*

Low temperature – high pressure behaviour of $LaPO_4 \cdot xH_2O$ was investigated with other SPS *in situ* dilatometry tests from 25 °C to 425 °C under 400 MPa. Results are reported on Fig. 4.

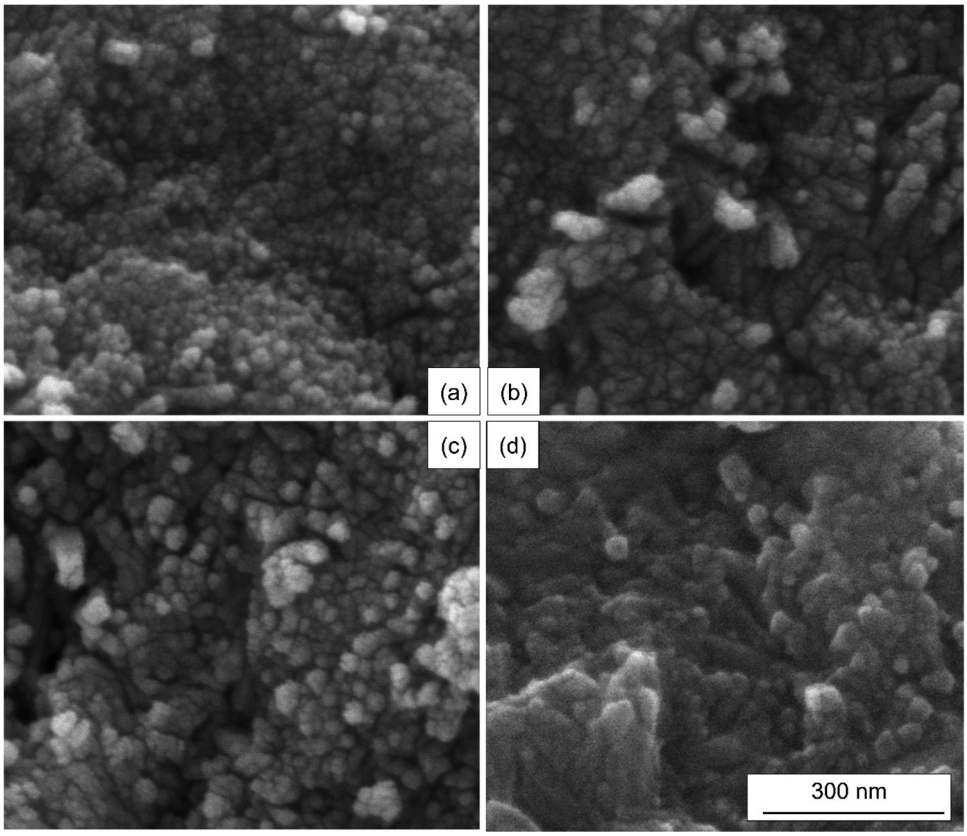


Fig. 6. SEM micrographs of (a) 160 °C, (b) 200 °C, (c) 260 °C and (d) 350 °C sintered $LaPO_4.xH_2O$.

During pressure application, no gas release is observed and an important shrinkage takes place. This first volume shrinkage is attributed to grains rearrangement. Once pressure reaches 400 MPa, temperature increases from 25 to 425 °C. From 25 to 190 °C shrinkage occurs with a negligible gas release. Above 190 °C, while shrinkage remains positive an important gas release is observed with a first peak at 230 °C and a second one at 320 °C represented by asterisks on Fig. 4. First, from 25 to 190 °C, shrinkage can be explained by the hydrated rhabdophane phase sintering. Above 190 °C, shrinkage interpretation is difficult due to gas release, which may also induce displacement. Thus, it is not possible to conclude on the origin of shrinkage behaviour (densification and/or gas elimination). Nevertheless, delayed water releases at 230 °C and 320 °C instead of 110 °C and 260 °C observed on TGA measurements indicate that applied pressure constrains water into the structure. It is confirmed by a clear gas release (represented by a cross on Fig. 4) induced by pressure removal at the end of experiment. Pressure induced water confinement has been reported for other compounds sintered in low temperature SPS [17].

To confirm and dissociate low temperature high pressure transformation steps, LPh has been sintered at 160 °C, 200 °C, 260 °C and 350 °C under 400 MPa during 10 min. X-Ray diffraction patterns of these samples are reported on Fig. 5.

Sample Spark Plasma Sintered at 160 °C exhibits its hydrated rhabdophane structure. These results confirm that the first shrinkage step (below 190 °C) corresponds to the sintering of rhabdophane phase. Monazite diffraction peaks appear at 200 °C while rhabdophane ones totally disappear at 260 °C. Phase transition appears to be related to the first gas release starting at 190 °C (Fig. 4). DTA measurements show endothermic behaviour up to 800 °C and literature data confirm the monazite phase formation up to 800 °C. Thus, pressure application has an influence on phase transition temperature, allowing monazite formation below 260 °C.

For all samples, XRD peaks width suggests a submicronic crystallite size. SEM observations made on sintered samples fracture are displayed on Fig. 6. They show nano-spherical grains with grain sizes below 50 nm. This is consistent with XRD peak broadening.

Sintered samples were further characterized to determine their skeletal densities by He pycnometry. Results are reported in Table 1. The 160 °C, 200 °C and 260 °C elaborated samples have lower skeletal densities than theoretical densities: 4.268 $g.cm^{-3}$ for rhabdophane [2] and 5.12 $g.cm^{-3}$ for monazite [30]. It can be partially explained by samples hydration (obtained via mass difference before and after drying at 500 °C during 2 h) which represents more than 1 wt.% for these samples. Nonetheless, considering its 1.3 wt.% hydration and the theoretical 5.12 $g.cm^{-3}$ monazite density, the 260 °C elaborated sample should have a higher density of 5.07 $g.cm^{-3}$ instead of 4.6 $g.cm^{-3}$. The

Table 1
Microstructure and properties of low temperature Spark Plasma Sintered lanthanum phosphate.

Sintering parameters			X-Ray given phase	Skeletal density (g. cm^{-3})	Hydration (wt.%)	Microhardness (GPa)
T (°C)	P (MPa)	t (min)				
160	400	10	rhabdophane	4.0	NA	1.3
200	400	10	mix	4.2	2.5	1.1
260	400	10	monazite	4.6	1.3	1.4
350	400	10	monazite	5.1	0.8	1.9

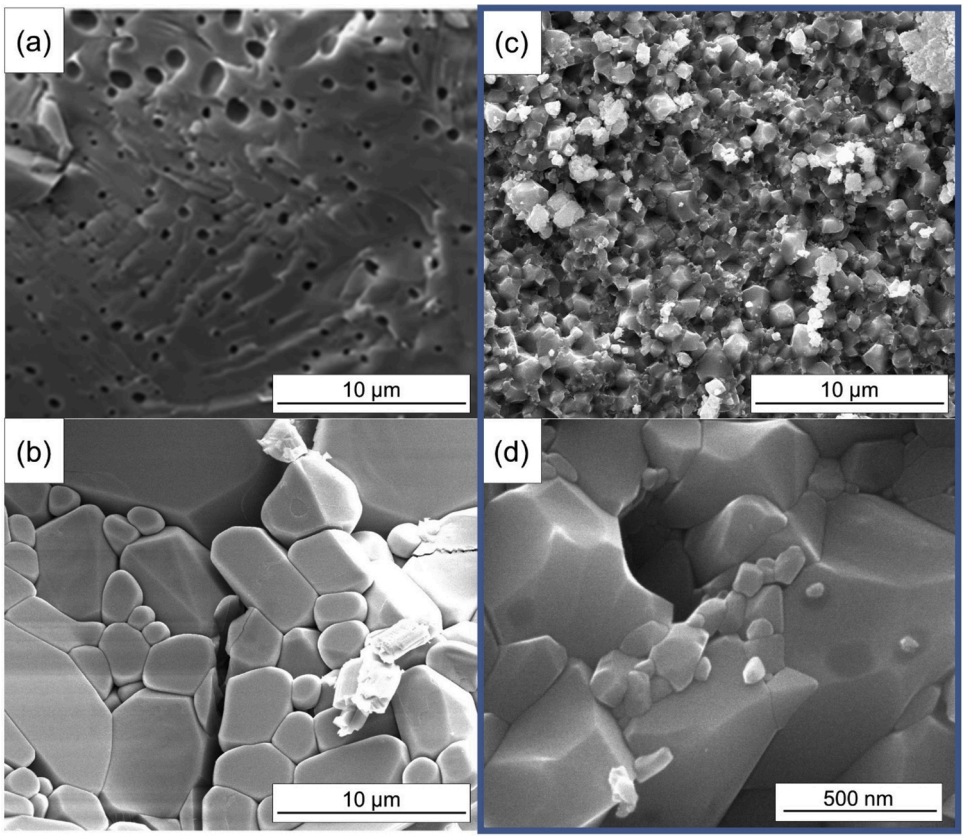


Fig. 7. Fracture surfaces SEM micrographs of (a) conventional sintered [27]; (b) Spark Plasma Sintered and (c-d) low temperature Spark Plasma Sintered LPh at 550 °C under 200 MPa (2 magnifications).

formation of an amorphous phase as intermediate step could explain the observed lower densities measured by pycnometry. Intermediate amorphous phase formation has already been observed on other compounds such as AlOOH [19] and seems usual for phosphated compounds [31].

Mechanical properties of these samples exhibiting grain sizes < 50 nm were measured by Vickers micro-hardness and reported in Table 1. Vickers Hardness increases with sintering temperature, which is consistent with the observed dehydration and crystallization of monazite structure sintered at higher temperature.

As shown previously, high applied pressure constrains water into the lanthanum phosphate structure. Thus, it limits low temperature monazite crystallization and results in hydrated sintered samples. To optimize monazite crystallization and full dehydration of sintered samples, we chose to decrease applied pressure to 200 MPa and increase sintering temperature up to 550 °C.

This new sintering cycle is compared in the following to a high temperature Spark Plasma Sintering (SPS) and a conventional sintering (CS) from literature.

Fig. 7 shows SEM images of $LaPO_4$ sintered from the hydrated precursor by various techniques (conventional (a), high temperature SPS (b) and low temperature reactive SPS at two magnifications (c & d)). Conventional sintering used by S.S. Sujith *etal.* [27] leads to a coarse microstructure with 15 µm grain size and closed segregated porosity (Fig. 7–(a)). This microstructure is characteristic of an advanced sintering along with important grain growth. Spark Plasma Sintering enables finer microstructures (Fig. 7-(b)) using high kinetics to avoid Ostwald ripening, grain size is 5 times smaller as compared to conventional sintering. Finally, low temperature Spark Plasma Sintering (Fig. 7-(c & d)) allows to further refine the microstructure with a bimodal grain size of 0.9 µm and 0.09 µm. Bimodality of grain size could be explained by dissolution-precipitation mechanisms inducing the appearance of nano-crystallites at grain boundaries [32].

As geometric densities are close to each other (Table 2), significant differences in the various mechanical behaviours can be pointed and explained. In fact, the coarse microstructure of CS sample has fully intragranular fracture mode with a low micro-hardness of 1.3 GPa while SPS and Low Temperature (LowT-SPS) samples exhibits an inter-granular fracture mode with an increased micro-hardness of, respectively, 2.3 ± 0.2 GPa and 2.5 ± 0.2 GPa. We can conclude that LowT-SPS, optimizing the temperature and pressure parameters to, respectively, 550 °C-200 MPa seems to be a good compromise to develop fine microstructures and to reach suitable mechanical properties as well.

Sintering from hydrated precursor allowed to use the dehydration

Table 2
Microstructures and properties of LPh elaborated by conventional sintering (CS), Spark Plasma Sintering (SPS) and low temperature Spark Plasma Sintering (LowT-SPS).

	Sintering parameters			Sample density	Grain size (µm)	Microhardness (GPa)	ref
	T (°C)	P (MPa)	t (min)	(g. cm^{-3})			
CS	1350	100	3h	4.7	15	1.3	[27]
SPS	1150	50	10 min	4.9	2.8	2.3	This study
LowT-SPS	550	200	10 min	4.8	0.9 & 0.09	2.5	

and phase transition as densification mechanisms. This low temperature evolutions, facilitated by applied pressure permits to achieve a well densified monazite-type lanthanum phosphate at temperature below 600 °C. In the same time, lower sintering temperature allows to avoid Ostwald ripening, leading to refined microstructures as compared to high temperature sintering processes. Finally, these refined microstructures cause an intergranular fracture mode that allows microhardness to reach values in the same range as those obtained on Spark Plasma Sintered lanthanum phosphate, but at temperature as low as 550 °C instead of 1150 °C.

4. Conclusion

The structural transition of lanthanum phosphate from rhabdophane to monazite phases was determined to occur in the range 150 °C–800 °C using XRD and TGA/DTA analyses. Sintering behaviour of rhabdophane and monazite phases were explored using Spark Plasma Sintering. While monazite densification ends at 1000 °C, it is shown that densification takes place below 600 °C from hydrated rhabdophane phase.

Several Low temperature Spark Plasma Sintering experiments on hydrated precursor were performed from 160 °C to 350 °C at a pressure of 400 MPa. Rhabdophane precursor hydration, stabilized by the 400 MPa applied pressure, is shown to help densification mechanisms through dehydration/phase transition starting at temperature as low as 200 °C. Yet, in these conditions, dehydration is incomplete and limits mechanical properties. For this reason, optimizing the parameters (T/P) is necessary to guarantee mechanical performances improvement. Thus, a densified sample, sintered at 550 °C under 200 MPa is obtained. It exhibits a submicronic bimodal (i.e. 0.09 and 0.9 μm grain sizes) microstructure which is finer than those obtained with conventional sintering and high temperature SPS. This submicronic and below 600 °C elaborated lanthanum phosphate achieves an up to 2.5 ± 0.2 GPa microhardness. For all these reasons, it is clearly shown that tuning the sintering parameters, this process is proved to open new opportunities for the elaboration of lanthanum phosphate.

Declaration of Competing Interest

The authors report no declarations of interest.

Acknowledgments

We thank Safran Aircraft Engines for the technical and financial support. The SPS experiments were performed at the Plateforme Nationale CNRS de Frittage-Flash (PNF2/CNRS Toulouse).

This work was supported by the association Nationale Recherche Technologie (ANRT) as part of the CIFRE (Industrial Agreement of Formation by Research) contract n°2018/1521.

References

[1] L. Perrière, D. Bregiroux, B. Naitali, F. Audubert, E. Champion, D.S. Smith, D. Bernache-Assollant, Microstructural dependence of the thermal and mechanical properties of monazite $LnPO_4$ (Ln=La to Gd), J. Eur. Ceram. Soc. (2007) 3207–3213, https://doi.org/10.1016/j.jeurceramsoc.2006.12.005.

[2] S. Lucas, Synthèse et comportement thermique (stabilité et frittage) de phosphate de terres rares cériques ou yttrique, thèse de doctorat, Université de Limoges, 2003.

[3] D.B. Marshall, P.E.D. Morgan, R.M. Housley, debonding in multilayered composites of zirconia and $LaPO_4$, J. Am. Ceram. Soc. (1997) 1677–1683, https://doi.org/10.1111/j.1151-2916.1997.tb03038.x.

[4] Y. Hikichi, T. Ota, T. Hattori, Thermal, mechanical and chemical properties of sintered monazite-(La, Ce, Nd or Sm), Miner. J. (1997) 123–130.

[5] R. Wang, W. Pan, J. Chen, M. Fang, Z. Cao, Y. Luo, Synthesis and sintering of $LaPO_4$ powder and its application, Mater. Chem. Phys. (2003) 30–36, https://doi.org/10.1016/S0254-0584(02)00420-0.

[6] A. Du, C. Wan, Z. Qu, R. Wu, W. Pan, Effects of texture on the thermal conductivity of the $LaPO_4$ monazite, J. Am. Ceram. Soc. 93 (2010) 2822–2827, https://doi.org/10.1111/j.1551-2916.2010.03779.x.

[7] A. Du, W. Pan, K. Ahmad, S. Shi, Z. Qu, C. Wan, Enhanced mechanical properties of machinable $LaPO_4/Al_2O_3$ composites by Spark Plasma Sintering, Appl. Ceram. Technol. (2009) 236–242, https://doi.org/10.1111/j.1744-7402.2008.02260.x.

[8] J.B. Davis, D.B. Marshall, R.M. Housley, P.E.D. Morgan, Machinable ceramics containing rare-earth phosphates, J. Am. Ceram. Soc. 81 (1998) 2169–2175, https://doi.org/10.1111/j.1151-2916.1998.tb02602.x.

[9] Q. Zheng, X. Wang, J. Tian, R. Kang, Y. Yin, Synthesis and characterization of $LaPO_4$ powder heat treated at various temperatures, Mater. Chem. Phys. (2010) 49–52, https://doi.org/10.1016/j.matchemphys.2010.03.002.

[10] J. Guo, R. Floyd, S. Lowum, J.-P. Maria, T. Herisson de beauvoir, J.-H. Seo, C. A. Randall, Cold sintering: progress, challenges, and future opportunities, Annu. Rev. Mater. Res. (2019) 275, https://doi.org/10.1146/annurev-matsci-070218-010041.

[11] F. Bouville, A.R. Studart, Geologically-inspired strong bulk ceramics made with water at room temperature, Nat. Commun. 8 (2017) 14655, https://doi.org/10.1038/ncomms14655.

[12] M. Biesuz, G. Taveri, A.I. Duff, E. Olevsky, D. Zhu, C. Hu, S. Grasso, A theoretical analysis of cold sintering, Adv. Appl. Ceram. 119 (2020) 75–89, https://doi.org/10.1080/17436753.2019.1692173.

[13] T.H. de Beauvoir, A. Sangregorio, I. Cornu, C. Elissalde, M. Josse, Cool-SPS: an opportunity for low temperature sintering of thermodynamically fragile materials, J. Mater. Chem. C 6 (2018) 2229–2233, https://doi.org/10.1039/C7TC05640K.

[14] S.H. Bang, T. Herisson De Beauvoir, C.A. Randall, Densification of thermodynamically unstable tin monoxide using cold sintering process, J. Eur. Ceram. Soc. 39 (2019) 1230–1236, https://doi.org/10.1016/j.jeurceramsoc.2018.11.026.

[15] M. Luginina, R. Orru, G. Cao, D. Grossin, F. Brouillet, G. Chevallier, C. Thouron, C. Drouet, First successful stabilization of consolidated amorphous calcium phosphate (ACP) by cold sintering: toward highly-resorbable reactive bioceramics, J. Mater. Chem. B 8 (2020) 629–635, https://doi.org/10.1039/C9TB02121C.

[16] J. Guo, X. Zhao, T.H.D. Beauvoir, J.-H. Seo, S.S. Berbano, A.L. Baker, C. Azina, C. A. Randall, Recent progress in applications of the cold sintering process for ceramic–polymer composites, Adv. Funct. Mater. 28 (2018), 1801724, https://doi.org/10.1002/adfm.201801724.

[17] T. Hérisson de Beauvoir, F. Molinari, U.C. Chung-Seu, D. Michau, D. Denux, M. Josse, Densification of $MnSO_4$ceramics by cool-SPS: evidences for a complex sintering mechanism and magnetoelectric coupling, J. Eur. Ceram. Soc. (2018) 3867–3874, https://doi.org/10.1016/j.jeurceramsoc.2018.04.005.

[18] M. Haug, F. Bouville, J. Adrien, A. Bonnin, E. Maire, A.R. Studart, Multiscale deformation processes during cold sintering of nanovaterite compacts, Acta Mater. 189 (2020) 266–273, https://doi.org/10.1016/j.actamat.2020.02.054.

[19] T. Hérisson de Beauvoir, C. Estournès, Translucent γ-AlOOH and γ-Al_2O_3 glass-ceramics using the cold sintering process, Scr. Mater. 194 (2020), 113650, https://doi.org/10.1016/j.scriptamat.2020.113650.

[20] J.-H. Seo, J. Guo, H. Guo, K. Verlinde, D.S.B. Heidary, R. Rajagopalan, C. A. Randall, Cold sintering of a Li-ion cathode: $LiFePO_4$-composite with high volumetric capacity, Ceram. Int. 43 (2017) 15370–15374, https://doi.org/10.1016/j.ceramint.2017.08.077.

[21] N. Guo, H.-Z. Shen, Q. Jin, P. Shen, Hydrated precursor-assisted densification of hydroxyapatite and its composites by cold sintering, Ceram. Int. 47 (2021) 14348–14353, https://doi.org/10.1016/j.ceramint.2021.01.294.

[22] T. Herisson de Beauvoir, V. Villemot, M. Josse, Cool-Spark Plasma Sintering: an opportunity for the development of molecular ceramics, Solid State Sci. 102 (2020), 106171, https://doi.org/10.1016/j.solidstatesciences.2020.106171.

[23] C. Elissalde, U.-C. Chung, M. Josse, G. Goglio, M.R. Suchomel, J. Majimel, A. Weibel, F. Soubie, A. Flaureau, A. Fregeac, C. Estournès, Single-step sintering of zirconia ceramics using hydroxide precursors and Spark Plasma Sintering below 400 °C, Scr. Mater. 168 (2019) 134–138, https://doi.org/10.1016/j.scriptamat.2019.04.037.

[24] E.E. Boakye, P. Mogilevsky, R.S. Hay, Synthesis of nanosized spherical rhabdophane particles, J. Am. Ceram. Soc. 88 (2005) 2740–2746, https://doi.org/10.1111/j.1551-2916.2005.00525.x.

[25] K. Rajesh, P. Shajesh, O. Seidel, P. Mukundan, K.G.K. Warrier, A facile sol–gel strategy for the synthesis of rod-shaped nanocrystalline high-surface-area lanthanum phosphate powders and nanocoatings, Adv. Funct. Mater. 17 (2007) 1682–1690, https://doi.org/10.1002/adfm.200600794.

[26] M. Yang, H. You, Y. Liang, J. Xu, F. Lu, L. Dai, Y. Liu, Morphology controllable and highly luminescent monoclinic $LaPO_4$:Eu^{3+} microspheres, J. Alloys. Compd. 582 (2014) 603–608, https://doi.org/10.1016/j.jallcom.2013.08.091.

[27] S.S. Sujith, S.L. Arun Kumar, R.V. Mangalaraja, A. Peer Mohamed, S. Ananthakumar, Porous to dense $LaPO_4$ sintered for advanced refractories, Ceram. Int. (2014) 15121–15129, https://doi.org/10.1016/j.ceramint.2014.06.125.

[28] V. Buissette, M. Moreau, T. Gacoin, J.-P. Boilot, J.-Y. Chane-Ching, T. Le Mercier, Colloidal synthesis of luminescent rhabdophane $LaPO_4$:Ln^{3+}·xH_2O (Ln = Ce, Tb, Eu; x ≈ 0.7) nanocrystals, Chem. Mater. 16 (2004) 3767–3773, https://doi.org/10.1021/cm049323a.

[29] D. Bregiroux, S. Lucas, E. Champion, F. Audubert, D. Bernache-Assollant, Sintering and microstructure of rare earth phosphate ceramics $REPO_4$ with RE=La, Ce or Y, J. Eur. Ceram. Soc. 26 (2006) 279–287, https://doi.org/10.1016/j.jeurceramsoc.2004.11.004.

[30] D.F. Mullica, W.O. Milligan, D.A. Grossie, G.W. Beall, L.A. Boatner, Ninefold coordination $LaPO_4$: Pentagonal interpenetrating tetrahedral polyhedron,

Inorganica Chim. Acta 95 (1984) 231–236, https://doi.org/10.1016/S0020-1693(1)87472-1.

MI. J. Vecstaudza, M. Gasik, J. Locs, Amorphous calcium phosphate materials: formation, structure and thermal behaviour, J. Eur. Ceram. Soc. 39 (2019) 1642–1649, https://doi.org/10.1016/j.jeurceramsoc.2018.11.003.

[32] J.-P. Maria, X. Kang, R.D. Floyd, E.C. Dickey, H. Guo, J. Guo, A. Baker, S. Funihashi, C.A. Randall, Cold sintering: current status and prospects, J. Mater. Res. 32 (2017) 3205–3218, https://doi.org/10.1557/jmr.2017.262.